MICHIGAN STATE UNIVERSITY

CYCLOTRON LABORATORY

(p, n) ISOBARIC ANALOG TRANSITIONS IN TARGETS OF ^{27}Al, ^{51}V, AND ^{90}Zr AT 22, 30 AND 40 MeV

R.K. JOLLY, T.M. AMOS, A. GALONSKY,
R. HINRICHS and R. St. ONGE

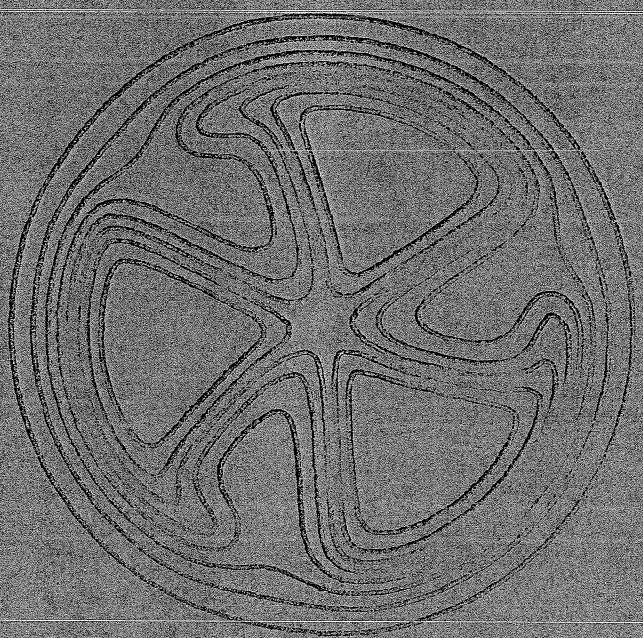

MSUCL – 76

JANUARY 1973

(p,n) Isobaric Analogue Transitions in Targets of ^{27}Al, ^{51}V, and ^{90}Zr at 22, 30, and 40 MeV*

R.K. Jolly,+ T.M. Amos,++ A. Galonsky,
R. Hinrichs,+++ and R. St. Onge++++

Cyclotron Laboratory, Physics Department
Michigan State University, East Lansing, Michigan 48823

ABSTRACT

Angular distributions for (p,n) transitions to isobaric analogue states of ^{27}Al, ^{51}V, and ^{90}Zr targets have been measured at proton energies of 22, 30, and 40 MeV. The data have been compared with results of macroscopic distorted waves Born approximation calculations employing various form factors: pure volume, pure surface, and mixtures of real volume with imaginary surface. The comparisons show that: i) the surface interaction describes the data rather well, particularly at the lower energies, whereas the volume interaction is adequate only at 40 MeV; ii) complex mixtures of volume and surface give good descriptions of most of the data if the mixture is a variation of the isospin part of the Becchetti-Greenlees potential with either increased surface-to-volume ratio or increased imaginary radius;

---

* Work supported by the National Science Foundation and the Office of Naval Research.

+ Present address: College of William and Mary, Virginia Associated Research Campus, Newport News, Virginia 23606

++ Present address: Resources Development Corp.,Okemos, Michigan 48864

+++ Present address: State University College Oswego, New York 13126

++++ Present address: University of New Hampshire, Durham, New Hampshire

iii) use of the unmodified Becchetti-Greenlees geometry gives a poor fit to much of the data; iv) the strength of the isospin interaction decreases with increasing energy, in general agreement with other charge-exchange work. Most of the decrease here occurs between 22 and 30 MeV. This is true for the surface interaction and for each of the two complex interactions.

I. INTRODUCTION

In (p,n) transitions between isobaric analogue states (IAS) the isospin interaction may be the main, in many cases the total, interaction causing the transition. Consequently, the most direct manner of studying the isospin interaction is through these transitions. Several such studies[1-5] have been reported, but there is as yet no clear cut indication of underlying simplicities or systematics in the interaction. The earlier studies, reviewed by Satchler,[6] have raised questions as to the radial form of the isospin interaction, that is, whether or not it is surface peaked. Also, there is very little evidence as to whether the interaction must be complex[7] or energy dependent.[8,9,10] To answer such questions will likely require a rather thorough study in which a wide range of target nuclei and proton bombarding energies are employed.

We describe here the measurements and analyses of (p,n) transitions to ground-state analogues of the target nuclei ^{27}Al, ^{51}V, and ^{90}Zr at incident proton energies of 22, 30, and 40 MeV. The experimental angular distributions were compared with macroscopic distorted waves Born approximation (DWBA) calculations employing both a real (volume or surface-peaked) and a complex isospin interaction. Since the interaction was taken to be spherically symmetric, only monopole transitions were used in the calculations for both even -A and odd -A targets.

II. EXPERIMENTAL PROCEDURE

Thin targets of ^{27}Al(6.2 mg/cm^2), ^{51}V(7.9 mg/cm^2), and 97.8% enriched ^{90}Zr (2.0 mg/cm^2) were bombarded with protons from the Michigan State University Cyclotron. The resulting neutron spectra were measured with a time-of-flight system[11] which makes use of the natural bunching of the cyclotron beam pulses. The neutron detector is the liquid scintillator NE-213, deoxygenated and encapsulated in a 2" diameter x 3/4" thick glass cell mounted on an RCA-8575 photomultiplier. Start and stop timing signals are derived from a constant-fraction discriminator on the photomultiplier and from the cyclotron rf voltage through a divide-by-2 scaler, respectively.

Two-dimensional pulse-shape analysis is used to distinguish neutrons from gamma rays. A typical neutron, γ-ray oscilloscope display is shown in Fig. 1, where the abcissa is pulse height and the ordinate is pulse shape, i.e., a timing signal derived from the shape of the light pulse. Mathematical boundaries are put around the two groups so that each event can be classified as "neutron" or "γ-ray" and its time of flight incorporated into the appropriate spectrum being accumulated in the computer memory. A typical γ-ray suppression-factor obtained with the system is 200.

In order to reduce background, the proton beam was refocused with a quadrupole triplet after it passed through the target and was transported 11 meters downstream into a heavily-shielded graphite beam dump. That portion of the beam (up to $\sim$10%) which

was scattered by the target to angles exceeding the acceptance of the lens was a serious source of background. In order to reduce this background the aluminum beam pipe was shielded internally from the scattered protons by graphite rings, and the graphite rings were externally shielded with lead and concrete. In addition, the detector was inside a steel-and-water shield.

Samples of time-of-flight spectra obtained at 30 MeV are shown in Figs. 2 and 3 for the ^{27}Al and ^{90}Zr targets, respectively. By causing the stop pulse for the time-to-amplitude converter to occur at a repetition rate which is one-half of the beam pulse rate, a given time of flight appears twice in the spectrum at pulse heights which differ by an amount corresponding to the beam repetition period, 61.8 nsec at 30 MeV. In each figure the width of the IAS peak, the most prominent neutron group, is 0.4 nsec FWHM, corresponding to a neutron energy resolution of approximately 0.4 MeV. The large peak in each γ-ray spectrum was produced by γ rays coming from the target. In order to avoid the confusion of a spectrum containing IAS neutrons overlapping lower-energy neutrons produced by an earlier beam pulse, signals from the latter source were suppressed by pulse-height selection. The spectrum in the region of suppression (channels 360 to 480 and 860 to 980) is a measure of the magnitude of the time-uncorrelated background.

When the incident proton energy was 22 or 30 MeV, the resolution achieved at a flight path of 2.5 meters was generally adequate to resolve the IAS group. At 40 MeV and for some of the

22- and 30- MeV runs longer flight paths were used. This was particularly necessary for 40-MeV runs with the aluminum target where the IAS was not completely resolved from the first two excited states of ^{27}Si at 0.78 and 0.96 MeV. The situation seen in Fig. 2, where the two excited states appear as a very small shoulder on the left side of the IAS peak, is typical. In order to check that we were correctly estimating the intensity contribution of the excited states, several runs were taken with flight paths up to 10 meters in length. A spectrum obtained at 10 meters is shown in Fig. 4. The IAS is clearly resolved from the excited states; indeed, the first two excited states are almost resolved from each other. Not all of the data could be taken at 10 meters because the geometry of the experimental room restricted such flight paths to the forward direction. Furthermore, the duration of a run would be unnecessarily long at 10 meters. At 2.5 meters a typical run time was a half hour.

The angular range covered in the experiment was 10° to 102.5°. The detector with its shield was mounted on a commercial air pad that could easily be moved when changing the observation angle or the flight path.

Because of the previously-discussed loss of beam through scattering in the target, the product of target thickness with incident flux was determined for each run from a 90° proton elastic scattering measurement and its known and/or calculated (via optical-model potentials) cross section. The efficiency of the

NE-213 neutron detector was determined by a computation with our version of Kurz's code.[12] Comparisons with experiment[12,13] indicate a ±10% accuracy for this code. Each point of our measured angular distributions should have a relative accuracy determined by the counting statistics of the IAS peak and the error in subtracting the background of other states under the IAS peak. Error bars on the data in the figures to follow, Figs. 5-8, are of this origin. In addition, each angular distribution is estimated to have an absolute uncertainty of ±20%. Our results for ^{27}Al at 30 MeV and for ^{51}V at 22 MeV are in agreement with the data of Batty et al.[2] and of Anderson et al.,[14] respectively. The Colorado group[3] measured (p,n) reactions on many targets, including ^{27}Al and ^{90}Zr, at 23 MeV. Compared to our 22-MeV data, their ^{27}Al data are approximately the same but their ^{90}Zr angular distributions agrees only at forward angles and falls off more rapidly with increasing angle; from 70° to 100° their cross sections are less than one-half of ours. Whether this discrepancy implies experimental error or a surprising energy dependence is not known.

III. COMPARISON OF RESULTS WITH DWBA CALCULATIONS

A. Radial Shape of the Isospin Interaction

By using the computer codes JULIE[15] and DWUCK[16] we have compared the measured angular distributions with DWBA calculations and the monopole collective model[17] of IAS excitations in direct

(p,n) reactions. To keep the analysis simple we first tried fitting the data with either a pure volume or a pure surface interaction. Then we combined the two forms into an interaction consisting of a real volume term and an imaginary surface term.

1. Pure Surface or Pure Volume Interaction

In the pure volume calculations the isospin part of the generalized nucleon-nucleus potential[18] is assumed to have the same shape (Woods-Saxon) as the real (volume) isoscalar part. The combined real potential is then

$$U(r)=-(e^{X_R}+1)^{-1}\ (V_o+4\frac{V_1\ \vec{t}\cdot\vec{T}}{A}\ ),$$

where $X_R=\frac{r-R}{a}$ and $\vec{t}$ and $\vec{T}$ are the nucleon and nucleus (mass A) isospins, respectively. The (p,n) cross section to the IAS is proportional to V_1^2.

In the pure surface calculations the isospin-dependent part of the potential is

$$U_1(r)=4W_1\ \frac{d}{dX_R}\ (e^{X_R}+1)^{-1}4\frac{\vec{t}\cdot\vec{T}}{A}\ .$$

The (p,n) cross section to the IAS is proportional to W_1^2.

For each energy and target two different nucleon-nucleus optical potentials were used in separate calculations. One potential was, in each case, a Becchetti-Greenlees potential.[19] For the other potential we used the parameters of Perey[20] for the protons and of Perey and Buck[21] for the neutrons in the calculations at 22 and 30 MeV. At 40 MeV we used the proton potentials of Fricke et al.[22]; corresponding neutron potentials were derived from these by reversing

the sign of the symmetry term and, of course, omitting the Coulomb potential. In view of the non-negligible (p,n) reaction Q values for all targets, the dependence of the potentials on neutron energy was taken into account. The values of the potential parameters used are in Tables I, II, and III for ^{27}Al, ^{51}V, and ^{90}Zr, respectively.

In Fig. 5 the data on ^{27}Al have been compared with DWBA calculations using the pure surface and the pure volume form factors for the isospin interaction. It is apparent that none of the volume calculations reproduces the shape of the experimental cross sections very well. The surface interaction, however, reproduces the shapes of the 30- and 40- MeV angular distributions rather well. At 22 MeV there is more structure in the calculations than in the data. At all three energies the surface form factor describes the data much better than does the volume form factor.

A similar comparison is given in Fig. 6 for the ^{51}V data. At all bombarding energies the surface interaction reproduces most of the structure in the angular distributions. The volume interaction, however, does not show any of the structure present in the 22- and 30- MeV data, but it agrees quite well with the 40- MeV data.

In the case of ^{90}Zr, Fig. 7, the 22- and 30- MeV data are well desceibed by the surface-interaction calculations, particularly with the potential parameters of Perey. At 40 MeV neither potential gives a good fit when the surface interaction is used, but a volume interaction fits rather well. Just 10 MeV lower, at 30 MeV, there are pronounced oscillations in the angular distributions, but the volume interaction predicts none and produces the poorest of all the fits presented thus far.

At 22 MeV the volume interaction also fails to predict the observed, although lessened, oscillation.

The for nine angular distributions measured the surface interaction gives a fairly good fit throughout. This general conclusion is independent of the optical potential used. The volume interaction gives an acceptable fit in only two cases, ^{51}V and ^{90}Zr at 40 MeV. Both the volume and surface form factors used the geometry of the real proton well. No overall improvement resulted when the radius of the form factor was changed.

2. Combined Volume and Surface Interaction

In attempting to get better fits by combining the surface and volume form factors, we were guided by recent reports[7,23] favoring a complex form factor of real volume and imaginary surface terms; that is, an isospin potential of the form

$$U_1(r)=[-V_1 f(X_R)+i4W_1 \frac{d}{dX_I} f(X_I)]\ 4\frac{\vec{t}\cdot\vec{T}}{A} .$$

In our calculations the geometrical parameters of the Woods-Saxon functions $f(X_R)$ and $f(X_I)$ were initially taken to be those of the Becchetti-Greenlees best fit, viz. r=1.17 F, a=0.75 F, r_I=1.29F (an average between the proton and neutron values of 1.32 F and 1.26 F, respectively), and a_I=0.58 F. The values of V_1 and W_1 in the above analysis are 24 MeV and 12 MeV, respectively; hence V_1/W_1=2. The Becchetti-Greenlees potential, Tables I-III, was also used to generate the proton and neutron distorted waves for the DWBA. The results of the calculation are dotted curves in Fig. 8. They do not reproduce the oscillations in the 30- MeV data, and are somewhere between the pure surface and pure volume in general goodness of fit.

In seeking a better fit to the data, many parameters of the DWBA could be varied. Recent studies of (^{3}He,t) reactions to IAS[24,25] find that the DWBA calculations are most sensitive to the imaginary surface term of the form factor. Based upon this we selected two parameters, the radius parameter r_I of the imaginary well and the ratio of volume to surface interaction strength V_1/W_1, through which to vary the imaginary surface term of the form factor. In all of these calculations the proton and neutron distorted waves were obtained from the unmodified Becchetti-Greenlees potential.

When all parameters except r_I were held fixed, the best overall fit for the 9 angular distributions was obtained with r_I=1.35 F. The results of these calculations are the dashed curves of Fig. 8. At 30 and 40 MeV there are now oscillations that match the data, but for ^{27}Al the calculated curves fall too rapidly with angle. At 22 MeV there is no improvement; the calculated curves, particularly for ^{27}Al, have too much structure. By increasing the radius parameter of the real well from r=1.17 F to r=1.27 F and restoring r_I to its Becchetti-Greenlees value of 1.29 F, it was possible to improve the fits to the 22- MeV data, but the same form factor then yielded too little structure to match the ^{51}V and ^{90}Zr data at 30 and 40 MeV. In varying r_I we found no evidence, in contrast to the analysis of 22.8- MeV data,[23] of a dependence of r_I on target mass. In fact, the suggested geometries of Ref. 23 gave poor fits to our 30- and 40- MeV data.

The other parameter of the imaginary, surface term to which the calculations are sensitive is the ratio V_1/W_1. By varying

this from the Becchetti-Greenlees value of 2, we found a good fit to the 30- and 40- MeV data by setting $V_1/W_1=2/3$ and keeping the geometry of the Becchetti-Greenlees potential; the 22- MeV calculations once again had more structure than the data. The results are shown in Fig. 8 by the solid curves. These are the best overall fits with a complex potential since they do a much better job on the 30- and 40- MeV ^{27}Al data than either of the other two fits.

Although a change in r_I from 1.29 F to 1.35 F produced sizeable, for ^{90}Zr at 30 MeV dramatic, changes in the DWBA result, the calculations were insensitive to changes of $\pm$0.1 F in a_I.

We also varied other parameters of the form factor and found, in agreement with the (^{3}He,t) work, that the calculations were less sensitive to their values.

B. Strength of the Isospin Interaction

As is apparent from Figs. 5-7 and 8 most of the nine measured angular distributions can be fitted with a pure surface interaction or with either of two simple modifications of the Becchetti-Greenlees complex mixture of surface and volume interactions. We can examine the strength of the isospin interaction in a meaningful way within the confines of a single geometry, i.e. radial dependence, of the interaction. Regardless of which geometry is used, we could hope to extract, however, the same trend of strength with proton energy and with target mass.

Strengths were obtained by equating the calculated and measured cross sections. Since these two never have exactly the same angular distribution, the equating is done to a part of or an integral of the angular distribution. For the pure surface interactions we used an integral over the angular range 10° to 92° or 102°. For the volume-plus-surface interactions we equated the forward-angle parts of the angular distributions because the 30- and 40- MeV ^{27}Al data were matched by the calculations up to 50° or 60°, but not beyond, where there is a large solid angle. As long as there is reasonable agreement in the shape of the angular distribution either method gives about the same value for the strength. Our best illustration of where this would not be true is the data of ^{90}Zr at 30 MeV "fitted" with the interaction geometry of the unmodified Becchetti-Greenlees potential--dotted curve in Fig. 8. Depending upon the details of matching one could, in this case, obtain almost a factor-of-two variation in the strength obtained.

Because of the lack of agreement with measured angular distributions in calculations with the unmodified Becchetti-Greenlees potential, strengths were not obtained for this potential.

For all of the other fits shown in Figs. 5-8 the surface strengths, W_1, are given in Table IV and Fig. 9. For the combined volume and surface interactions V_1 is either 2/3 W_1 or 2 W_1 as indicated. Although specific errors are not assigned to the strengths, it should be remembered that the absolute values of the cross sections are uncertain to $\sim^{\pm}$20% and a strength is proportional to the square root of the cross section, hence uncertain
$\sim^{\pm}$10%.

Although three different geometries were used to obtain the strengths, it is clear from Fig. 9 that the trend with energy and target is generally the same in all three cases. In particular, there is always a decrease between E_p=22 and 30 MeV, and at each energy the strength for ^{51}V is always less than the strengths for ^{27}Al and ^{90}Zr.

Decreasing strengths between 30 and 50 MeV have been found by Wong et al.[7] in analyzing data of Batty et al.[2] with the Becchetti-Greenlees potential. A decrease has also been observed in analysis of (p,n) total IAS cross sections with targets of ^{91}Zr, ^{119}Sn, ^{208}Pb and ^{209}Bi between ∿25 and 45 MeV.[8,9,10] The data of Thurlow[26] at 94 MeV requires a strength only ∿1/4 that needed at 18 MeV.[6] Even in (^3He,t) measurements to IAS[24,25] there is a large decrease in strength over the range of the measurements, 21 to 70 MeV. Although compound nucleus effects decrease in importance with increasing energy, experience would indicate that they would already be negligible at 20 MeV. Certainly this is true of compound elastic scattering, which is closely related to compound IAS production. Another possibility for understanding the decreasing strengths is that the radial shape of the charge-exchange interaction is changing with energy. There is some evidence for this in Figs. 5-7 in that the volume form factor is generally inadequate at 22 and 30 MeV, but gives a good fit to the ^{51}V and ^{90}Zr 40- MeV data. Perhaps the energy dependence of the strength of the surface form factor is a mere reflection of the energy dependence of the shape of the form factor.

If ambiguities are to be removed and systematics uncovered, there will have to be new measurements giving more detailed angular distributions at more closely spaced bombarding energies.

V. ACKNOWLEDGEMENTS

We are indebted to Professor Henry Blosser for assistance in setting up the neutron time-of-flight beam line and for help in obtaining very narrow beam bursts from the cyclotron. Also greatfully acknowledged is the cheerful assistance of Mary K. Zigrang, unfortunately now deceased, in the data reduction process.

REFERENCES

1. J.D. Anderson, C. Wong, J.W. McClure and B.D. Walker, Phys. Rev. 136, B118(1964).
2. C.J. Batty, B.E. Bonner, E. Friedman, C. Tschalar, L.E. Williams, A.S. Clough and J.B. Hunt, Nucl. Phys. A116, 643(1968).
3. R.F. Bentley, J.D. Carlson, D.A. Lind, R.B. Perkins and C.D. Zafiratos, Phys. Rev. Letters 27, 1081(1971).
4. A. Langsford, P.H. Bowen, G.C. Cox and M.J.M. Saltmarsh, Nuc. Phys. A113, 433(1968).
5. L. Valentin, Nuc. Phys. 62, 81(1964).
6. G.R. Satchler Ch. 9 in "Isospin in Nuclear Physics" edited by D.H. Wilkinson (North Holland Publishing Co.) 1969.
7. C. Wong, J.D. Anderson, J.W. McClure, B.A. Pohl, and J.J. Wesolowski, Phys. Rev. C5, 158(1972).
8. G.W. Hoffman, W.H. Dunlop, G.J. Igo, J.G. Kulleck, J.W. Sunier and C.A. Whitten, Jr., Nucl. Phys. A187, 577(1972).
9. T.J. Woods, G.T. Igo and C.A. Whitten, Jr., Phys. Letters, 39B, 193(1972).
10. G.W. Hoffman and W.R. Cohen, Phys. Rev. Letters 29, 22(1972).
11. R. St. Onge, T. Amos, A. Galonsky and R. Jolly, Bull. Am. Phys. Soc. 15, 1671(1970) and 16, 1172(1971).
12. Richard J. Kurz, Lawrence Radiation Laboratory Report, No. UCRL 11339(March 1964).
13. J.B. Hunt, C.A. Baker, C.J. Batty, P. Ford, E. Freidman and L.E. Williams, Nucl. Instr. Methods 85, 269(1970).

14. John D. Anderson, Bull. Am. Phys. Soc. 17, 527(1972) and private communication.

15. R.H. Bassel, R.M. Drisko and G.R. Satchler, Oak Ridge National Laboratory Report No. 3240 (Unpublished) and a subsequent memorandum to users of JULIE 1966 (Unpublished).

16. P.D. Kunz, Private communication.

17. G.R. Satchler, R.M. Drisko and R.H. Bassel, Phys. Rev. 136, B637(1964).

18. A.M. Lane, Nucl. Phys. 35, 676(1962).

19. F.D. Becchetti, Jr. and G.W. Greenlees, Phys. Rev. 182, 1190(1969).

20. F.G. Perey, Phys. Rev. 131, 745(1963).

21. F. Perey and B. Buck, Nuc. Phys. 32, 353(1962).

22. M.P. Fricke, E.E. Gross, B.J. Morton and A. Zuker, Phys. Rev. 156, 1207(1967).

23. J.D. Carlson, D.A. Lind and C.D. Zafiratos, preprint.

24. W.L. Fadner, J.J. Kraushaar and S.I. Hayakawa, Phys. Rev. C5, 859(1972).

25. R.A. Hinrichs and D.A. Show, Phys. Rev. C6, 1257(1972).

26. Nola Thurlow, Nucl. Phys. A109, 471(1968).

Table I. Optical-Model Parameters for $^{27}Al(p,n)$ Calculations. Energies are in MeV, distances in Fermis.

E_p	Potential	Particle	Energy	V	$r=r_c$	$a=a_{so}$	W_v	W_s	r_I	a_I	V_{so}	r_{so}
22	Perey[a]	p	22	43.5	1.25	.65	0	9.0	1.25	.47	8.5	1.25
		n	16.4	43.2	1.25	.65	0	10.0	1.25	.47	8.5	1.25
	Becchetti-Greenlees[b]	p	22	51.5	1.17	.75	8	8.3	1.32	.54	6.2	1.01
		n	16.4	50.0	1.17	.75	1.7	8.5	1.26	.58	6.2	1.01
30	Perey[a]	p	30	39.5	1.25	.65	0	7.5	1.25	.47	8.5	1.25
		n	24.4	40.8	1.25	.65	0	10.0	1.25	.47	8.5	1.25
	Becchetti-Greenlees[b]	p	30	48.9	1.17	.75	2.6	5.8	1.32	.54	6.2	1.01
		n	24.4	47.8	1.17	.75	3.7	6.5	1.26	.58	6.2	1.01
40	Fricke[c]	p	40	39.7	1.18	.70	7.0	0	1.40	.70	7.5	1.18
		n	34.4	38.0	1.18	.70	10.0	0	1.40	.70	7.5	1.18
	Becchetti-Greenlees[b]	p	40	45.7	1.17	.75	4.8	3.8	1.32	.54	6.2	1.01
		n	34.4	44.4	1.17	.75	6.9	4.1	1.26	.58	6.2	1.01

[a] See refs. 20 and 21.

[b] See ref. 19.

[c] See ref. 22.

Table II. Optical-Model Parameters for $^{51}V(p,n)$ Calculations. Energies are in MeV, distances in Fermis.

E_p	Potential	Particle	Energy	V	$r=r_c$	$a=a_{so}$	W_v	W_s	r_I	a_I	V_{so}	r_{so}
22	Perey[a]	p	22	46.0	1.25	.65	0	12.0	1.25	.47	8.5	1.25
		n	13.9	44.0	1.25	.65	0	10.0	1.25	.47	8.5	1.25
	Becchetti-Greenlees[b]	p	22	51.8	1.17	.75	2.1	7.5	1.32	.58	6.2	1.01
		n	13.9	46.9	1.17	.75	3.3	6.43	1.26	.58	6.2	1.01
30	Perey[a]	p	30	41.9	1.25	.65	0	11.1	1.25	.47	8.5	1.25
		n	21.9	41.4	1.25	.65	0	10.0	1.25	.47	8.5	1.25
	Becchetti-Greenlees[b]	p	30	49.2	1.17	.75	3.9	5.5	1.32	.58	6.2	1.01
		n	21.9	44.4	1.17	.75	5.0	4.33	1.26	.58	6.2	1.01
40	Fricke[c]	p	40	45.8	1.16	.75	6.9	1.14	1.37	.63	6.0	1.06
		n	31.9	40.3	1.16	.75	6.9	1.14	1.37	.63	6.0	1.06
	Becchetti-Greenlees[b]	p	40	46.0	1.17	.75	6.1	3.0	1.32	.58	6.2	1.01
		n	31.9	41.2	1.17	.75	7.2	1.83	1.26	.58	6.2	1.sl

[a] See refs. 20 and 21.

[b] See ref. 19.

[c] See ref. 22.

Table III. Optical-Model Parameters for $^{90}Zr(p,n)$ Calculations. Energies are in MeV, distances in Fermis

E_p	Potential	Particle	Energy	V	$r=r_c$	$a=a_{so}$	W_v	W_s	r_I	a_I	V_{so}	r_{so}
22	Perey[a]	p	22	47.7	1.25	.65	0	13.6	1.25	.47	8.5	1.25
		n	10.2	45.0	1.25	.65	0	10.0	1.25	.47	8.5	1.25
	Becchetti-Greenlees[b]	p	22	53.2	1.17	.75	2.1	7.26	1.32	.59	6.2	1.01
		n	10.2	46.6	1.17	.75	3.3	6.17	1.26	.58	6.2	1.01
30	Perey[a]	p	30	43.4	1.25	.65	0	13.4	1.25	.47	8.5	1.25
		n	18.2	42.6	1.25	.65	0	10.0	1.25	.47	8.5	1.25
	Becchetti-Greenlees[b]	p	30	50.6	1.17	.75	3.9	5.60	1.32	.59	6.2	1.01
		n	18.2	44.0	1.17	.75	5.0	4.17	1.26	.58	6.2	1.01
40	Fricke[c]	p	40	47.8	1.16	.75	4.7	3.45	1.37	.63	6.0	1.06
		n	28.2	40.8	1.16	.75	4.7	3.45	1.37	.63	6.0	1.06
	Becchetti-Greenlees[b]	p	40	47.4	1.17	.75	6.1	3.10	1.32	.59	6.2	1.01
		n	28.2	40.8	1.17	.75	7.2	1.67	1.26	.58	6.2	1.01

[a] See refs. 20 and 21.

[b] See ref. 19.

[c] See ref. 22.

Table IV. Surface strengths, W_I of the isospin interactions.

All units are MeV.

	^{27}Al	^{51}V	^{90}Zr	Form Factor
1. Pure surface interactions				
E_p=22	25.0	21.6	34.3	Surface, B-G[a] real geometry
30	18.2	13.8	24.1	Surface, B-G[a] real geometry
40	19.2	14.9	20.9	Surface, B-G[a] real geometry
22	23.2	19.8	26.4	Surface, Perey[b] real geometry
30	17.1	14.1	21.9	Surface, Perey[b] real geometry
40	19.6	15.7	22.0	Surface, Fricke[c] real geometry
2. Combined volume and surface interactions				
22	22.9	19.1	25.5	Real volume plus imaginary
30	20.2	12.8	21.8	surface, B-G[a] geometry
40	18.4	14.6	17.6	(r_I=1.29 F), but V_I=2/3 W_I.
22	8.7	7.0	9.8	Real volume plus imaginary
30	7.8	5.0	8.9	surface, B-G[a] strength mixture
40	7.5	6.0	6.6	(V_I=2W_I), but r_I=1.35 F.

a See ref. 19. B-G = Becchetti-Greenlees.

b See refs. 20 and 21.

c See ref. 22.

FIGURE CAPTIONS

Figure 1 Oscilloscope display of pulse-shape analysis used for neutron: γ-ray discrimination. The abcissa is light-output pulse height, the ordinate pulse shape, i.e., a timing signal derived from the shape of the light pulse. The dashed curves, which were set up by the experimenter with the aid of the computer, define an event as neutron or γ ray depending upon its location in the lower or upper band, respectively.

Figure 2 Typical time-of-flight spectra for 30-MeV protons on aluminum. The IAS group, for this target the ground-state group, peaks at channel 365 (and 865). Leakage of target γ-ray events, channel 605, into the neutron band is seen to occur about 0.5% of the time.

Figure 3 Typical time-of-flight spectra for 30-MeV protons on ^{90}Zr. The IAS group peaks at channel 320 (and 820).

Figure 4 Neutron time-of-flight spectrum for 31.75-MeV protons on aluminum. The flight path is 10 meters. At this distance the first-and second-excited states at 0.77 and 0.95 MeV, respectively, are cleanly separated from the ground (IAS) state. Compare with spectrum in Fig. 2 taken at 2.5 meters.

Figure 5 Differential cross sections for (p,n) to the IAS of the target ^{27}Al at proton bombarding energies of 22, 30, and 40 MeV. The data are presented twice, on the left for comparison with DWBA calculations employing a pure surface interaction and on the right for a pure volume interaction. The parameters of the potentials used are listed in Table I. All curves were normalized to the data.

Figure 6 Same as Fig. 5 except that target is ^{51}V and potential parameters are in Table II.

Figure 7 Same as Fig. 5 except that target is ^{90}Zr and potential parameters are in Table III.

Figure 8 The same data as in Figs. 5-7 compared with DWBA calculations employing an interaction consisting of a real volume part of strength V_1 and an imaginary surface part of strength W_1. The parameters were those of the Becchetti-Greenlees potential, ref. 19, for the dotted curves. For the dashed curves the parameters were the same except that r_I was increased from 1.29 to 1.35 F. For the solid curves r_I was returned to 1.29 F and V_1/W_1 was decreased from 2 to 2/3. All curves were normalized to the data. In all cases the distorted waves were generated with the Becchetti-Greenlees parameters listed in Tables I-III.

Figure 9 Surface interaction strengths W_1 vs proton bombarding energy E_p for the pure surface interactions of Figs. 5-7 (upper section) and two of the complex interactions of Fig. 8 (lower section). The straight lines connect points within the same interaction family.

Fig. 1

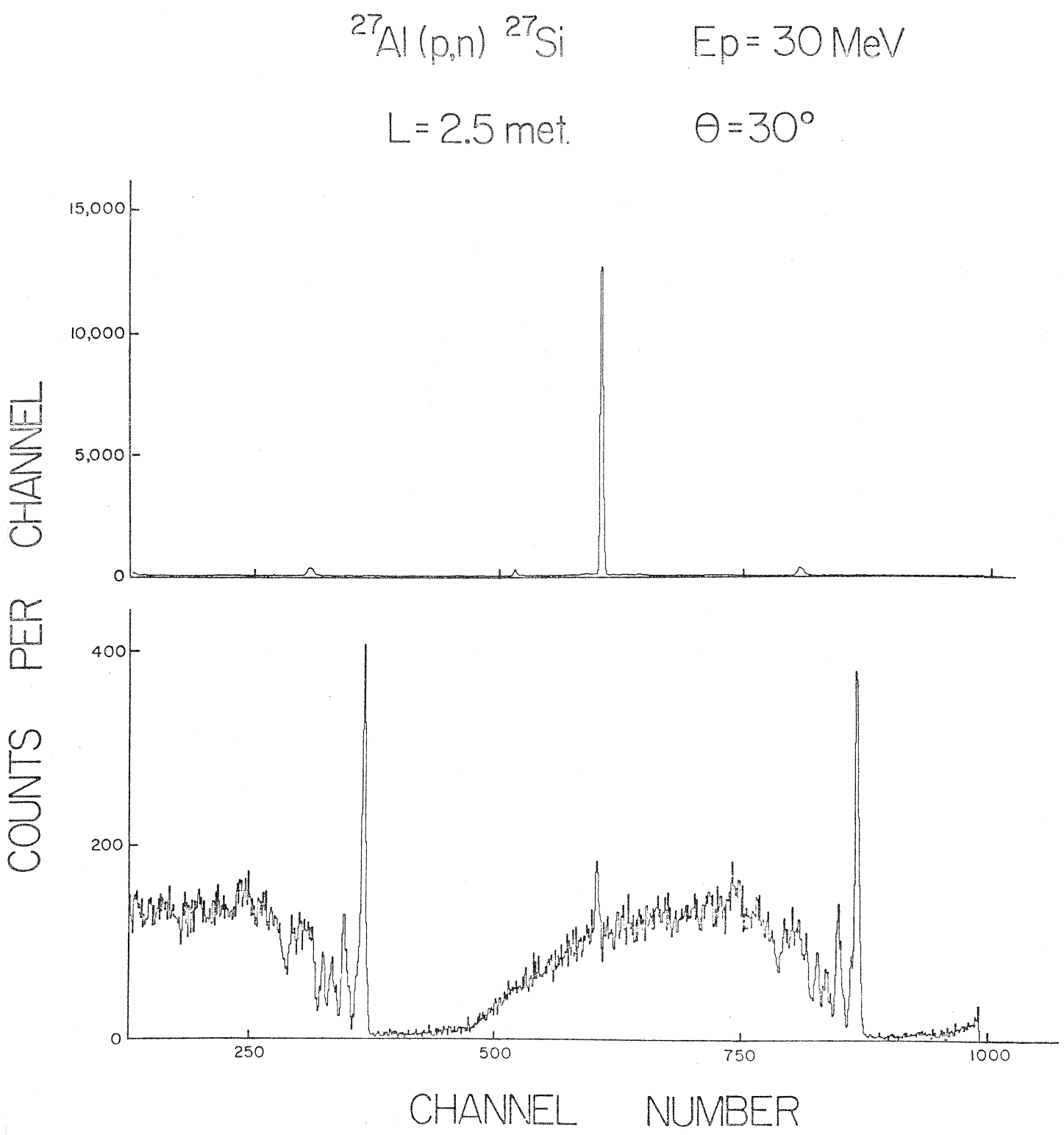
^{27}Al (p,n) ^{27}Si
Ep = 30 MeV
L = 2.5 met.
θ = 30°
15,000
10,000
5,000
0
400
200
0
250
500
750
1000
COUNTS PER CHANNEL
CHANNEL NUMBER

Fig. 2

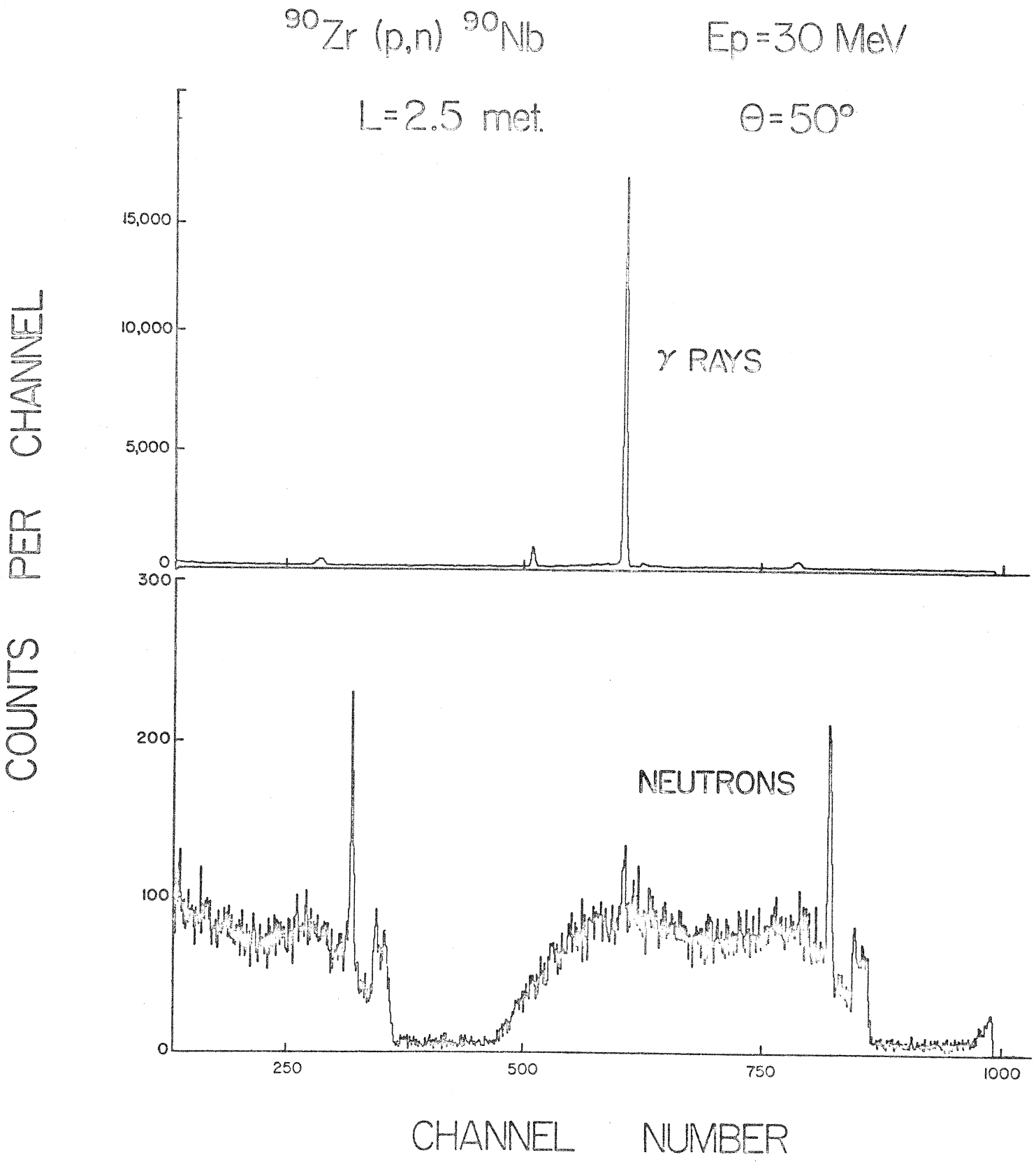
^{90}Zr (p,n) ^{90}Nb
Ep = 30 MeV
L = 2.5 met.
θ = 50°
15,000
10,000
5,000
0
γ RAYS
300
200
100
0
NEUTRONS
250
500
750
1000
COUNTS PER CHANNEL
CHANNEL NUMBER

Fig. 3

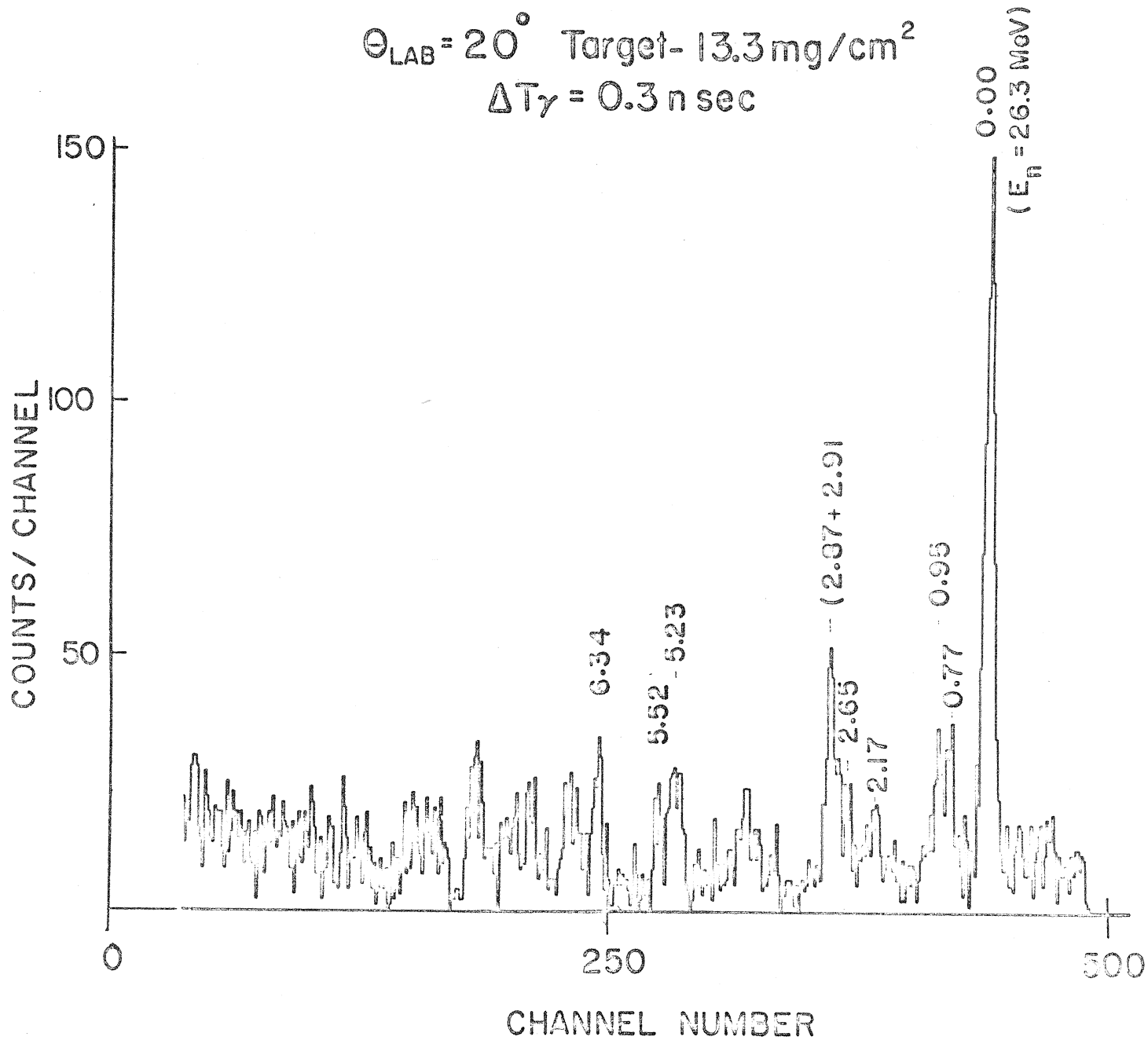
$^{27}Al(P,N)^{27}Si$ Ep = 31.75-MEV
$\theta_{LAB} = 20^{\circ}$ Target- 13.3 mg/cm^2
ΔT_γ = 0.3 n sec
0.00 (E_n = 26.3 MeV)
6.34
5.52 - 5.23
(2.87 + 2.91)
2.65
2.17
0.95
0.77
150
100
50
0
250
500
COUNTS/ CHANNEL
CHANNEL NUMBER

Fig. 4

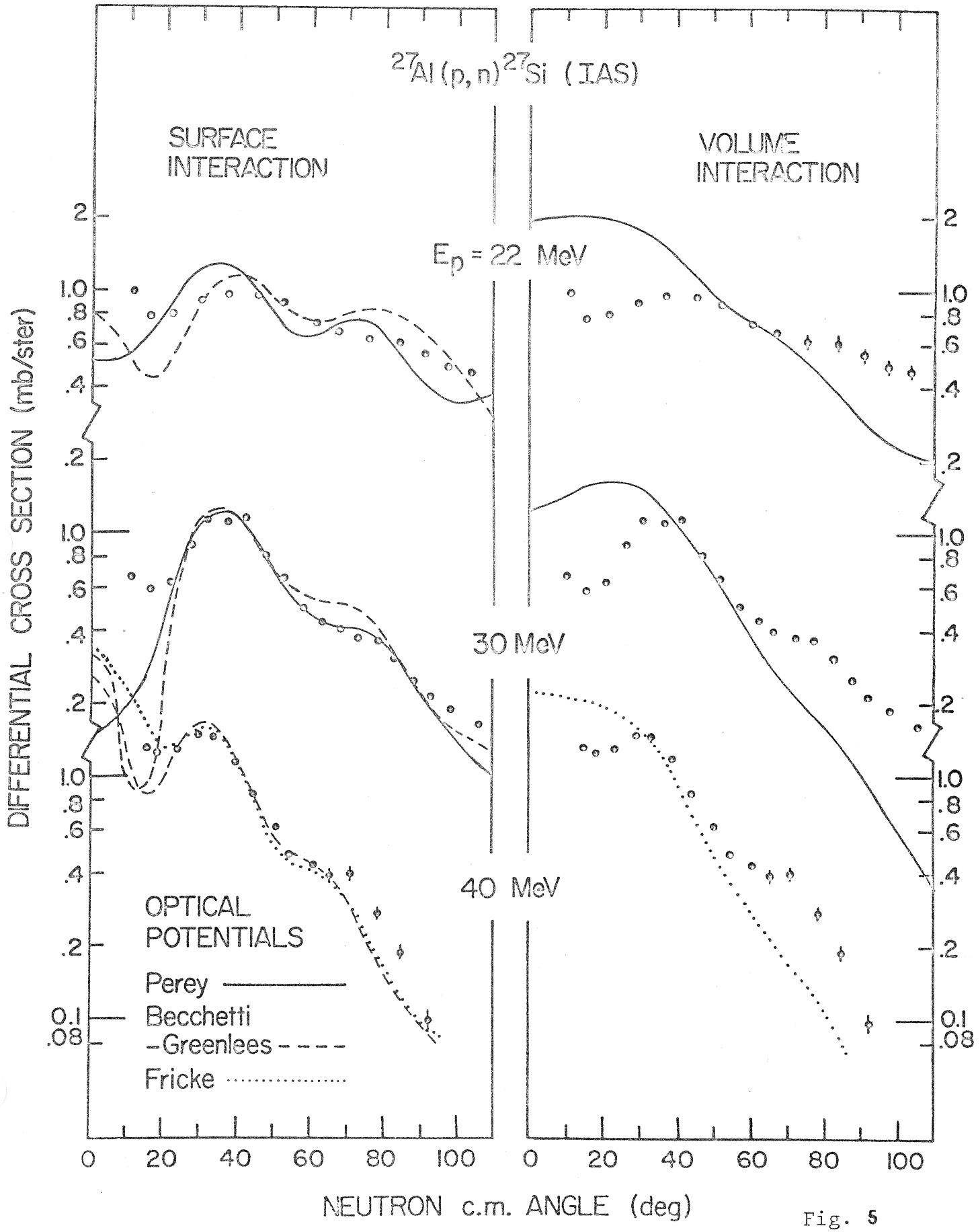
$^{27}Al(p,n)^{27}Si$ (IAS)
SURFACE INTERACTION
VOLUME INTERACTION
E_p = 22 MeV
30 MeV
40 MeV
OPTICAL POTENTIALS
Perey
Becchetti
Greenlees
Fricke
DIFFERENTIAL CROSS SECTION (mb/ster)
NEUTRON c.m. ANGLE (deg)
0 20 40 60 80 100
2 1.0 .8 .6 .4 .2 0.1 .08

Fig. 5

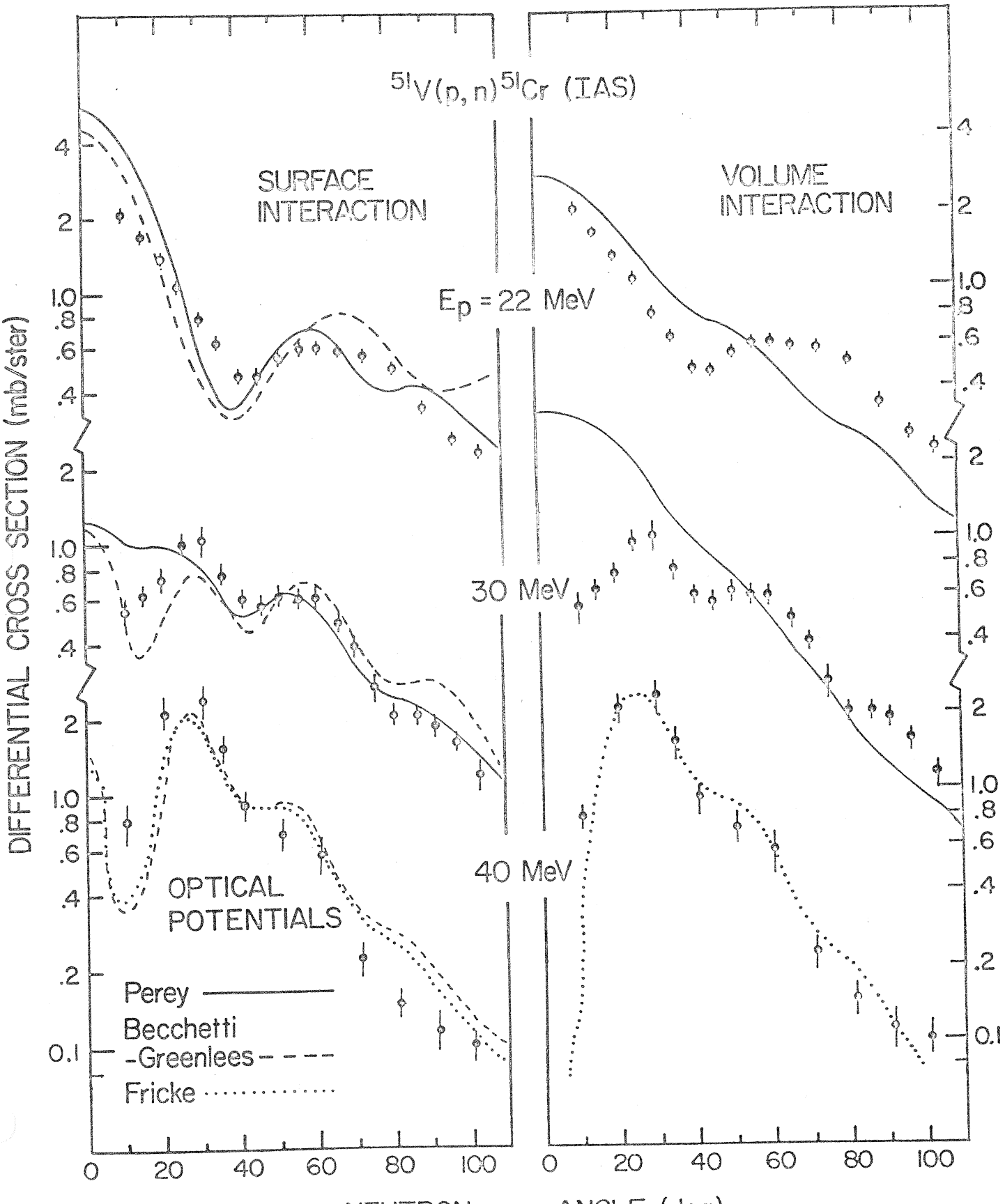
$^{51}V(p,n)^{51}Cr$ (IAS)
SURFACE INTERACTION
VOLUME INTERACTION
E_p = 22 MeV
30 MeV
40 MeV
OPTICAL POTENTIALS
Perey
Becchetti -Greenlees
Fricke
DIFFERENTIAL CROSS SECTION (mb/ster)
NEUTRON c.m. ANGLE (deg)

Fig. 6

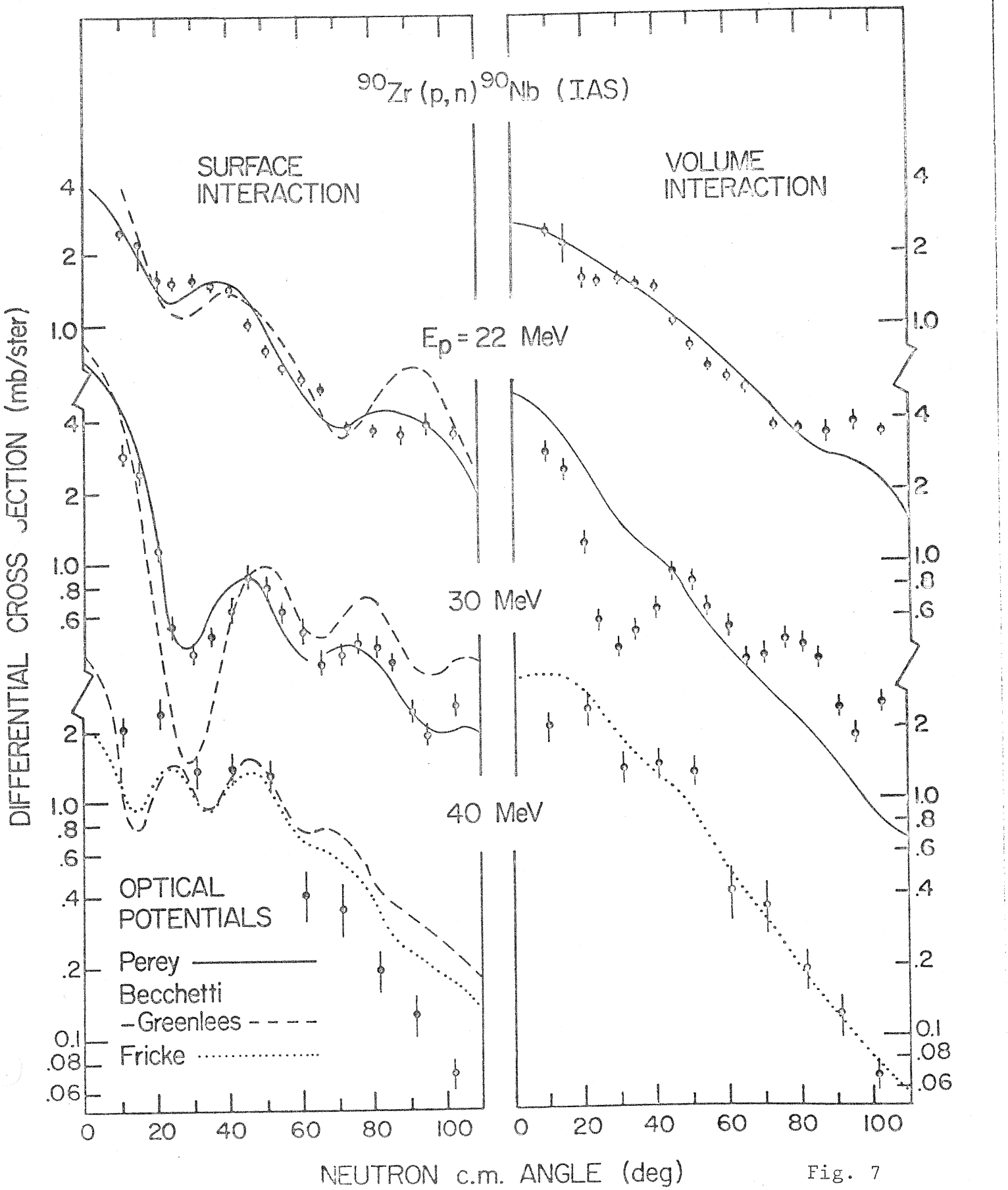
$^{90}Zr(p,n)^{90}Nb$ (IAS)
SURFACE INTERACTION
VOLUME INTERACTION
E_p = 22 MeV
30 MeV
40 MeV
OPTICAL POTENTIALS
Perey
Becchetti
Greenlees
Fricke
DIFFERENTIAL CROSS SECTION (mb/ster)
NEUTRON c.m. ANGLE (deg)
0
20
40
60
80
100

Fig. 7

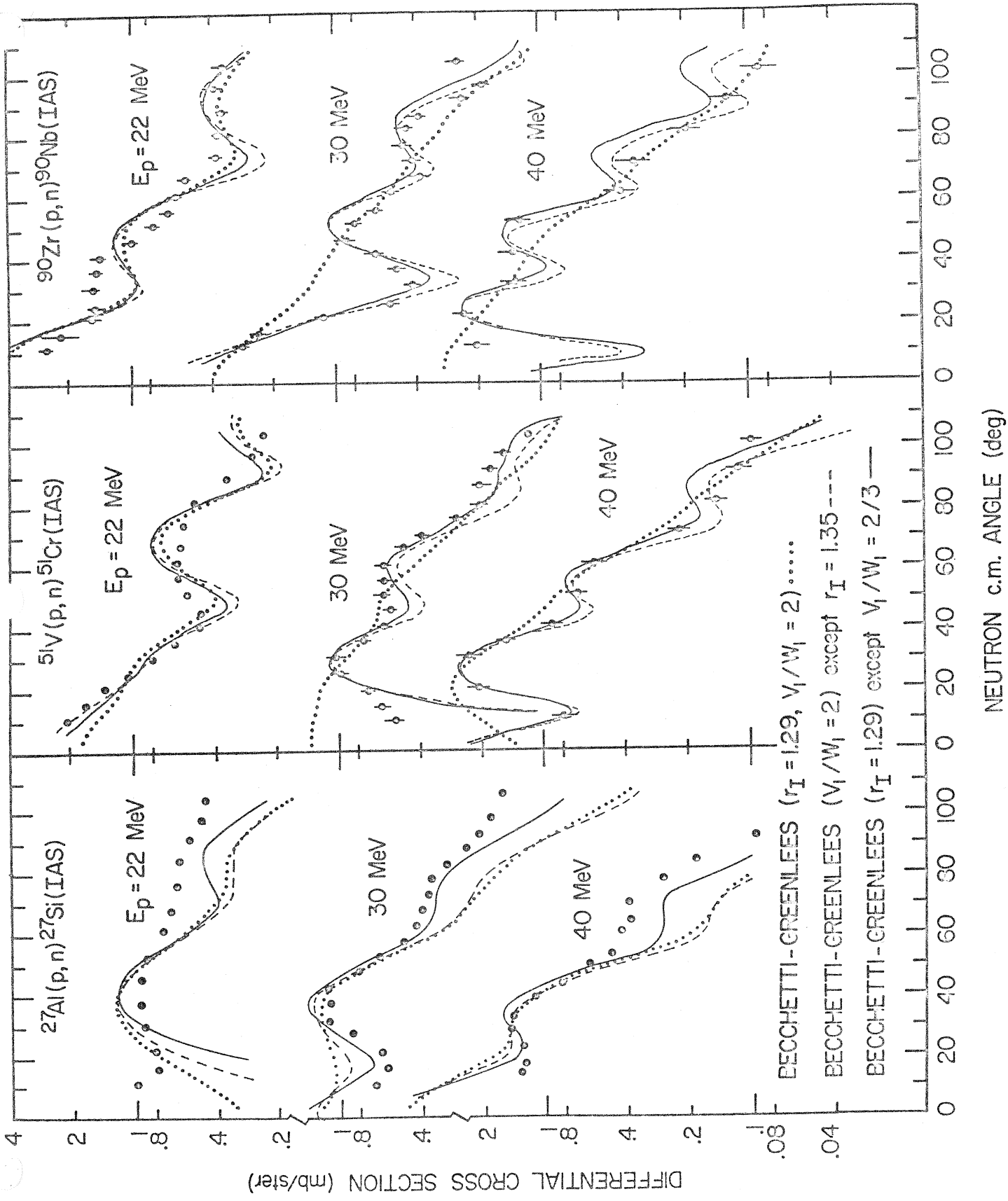
$^{27}Al(p,n)^{27}Si(IAS)$
$^{51}V(p,n)^{51}Cr(IAS)$
$^{90}Zr(p,n)^{90}Nb(IAS)$
E_p = 22 MeV
30 MeV
40 MeV
BECCHETTI-GREENLEES (r_I = 1.29, V_I/W_I = 2).....
BECCHETTI-GREENLEES (V_I/W_I = 2) except r_I = 1.35---
BECCHETTI-GREENLEES (r_I = 1.29) except V_I/W_I = 2/3 —
DIFFERENTIAL CROSS SECTION (mb/ster)
NEUTRON c.m. ANGLE (deg)

Fig. 8

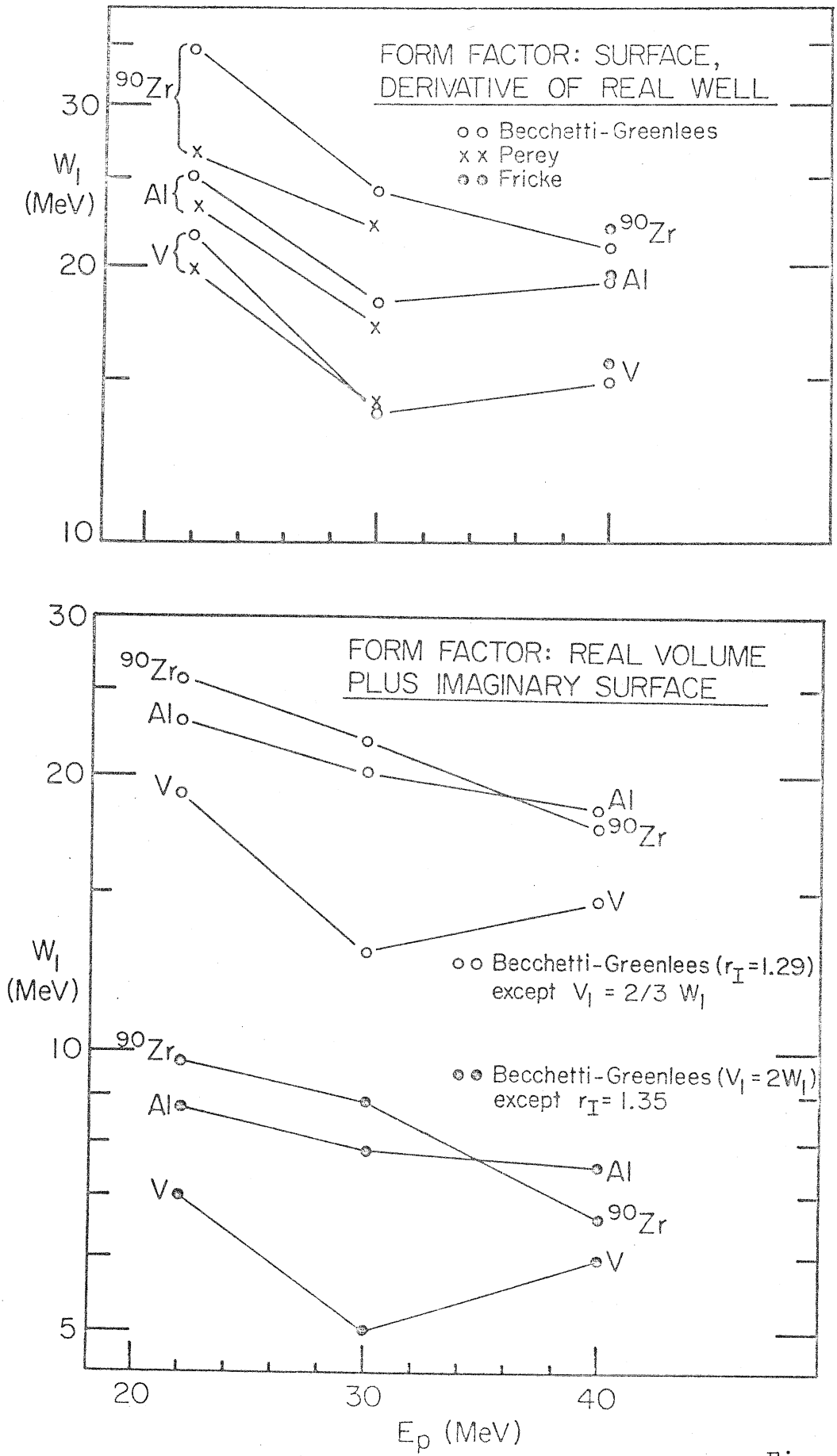
FORM FACTOR: SURFACE, DERIVATIVE OF REAL WELL
o o Becchetti-Greenlees
x x Perey
o o Fricke
90Zr
Al
V
30
20
10
W_I (MeV)
FORM FACTOR: REAL VOLUME PLUS IMAGINARY SURFACE
o o Becchetti-Greenlees (r_I = 1.29) except V_I = 2/3 W_I
o o Becchetti-Greenlees (V_I = 2W_I) except r_I = 1.35
30
20
10
5
20
30
40
E_p (MeV)

Fig. 9